4. NUMERICAL SIMULATION OF THE INDIAN SUMMER MONSOON

The climatology of the Indian summer monsoon presented in Chapter 2 describes the characteristic features of the monsoon circulation over India. It was shown (see Section 2.3) that a southwesterly current prevails in the lower troposphere and a marked easterly flow with a slightly southward component predominates in the higher levels. However, purely observational study alone would hardly help to explain the dynamics of the monsoon circulation itself. Investigations along theoretical and numerical lines based upon observations are necessary in order to understand the basic mechanism responsible for the development and the maintenance of the monsoon. An attempt has, therefore, been made to carry out a numerical experiment to simulate the Indian summer monsoon. As it is not feasible to have at the outset a complete and exhaustive treatment, it has been considered desirable to formulate a program of simplified models as sub-sets of the most general one. Such a less complex version may lack in itself detailed similitude to the monsoon but it provides the insight necessary for planning subsequently a more detailed scientific inquiry. The object of the present experiment, therefore, is to simulate the essential features of the monsoon circulation with a minimum of parametric constraints.

4.1 Numerical Simulation

Numerical simulation is a technique which is used to program controlled numerical experiments. It is the outgrowth of Numerical Weather Prediction (NWP) and consists of a time dependent system of equations like those of NWP. But unlike NWP, the initial conditions need not represent any actually observed state of the atmosphere and also the time over which the solution is extended could be months or even years rather than a day or a few days, so that a reasonably representative climatology is established. The solution is obtained by what is known as iterative or marching process. The solution is asymptotic in nature as schematically represented in Figure 4.1.1.

The feasibility of numerically simulating the general circulation was first demonstrated by Phillips (1956). Subsequently, Charney (1959), Smagorinsky (1963) and others (Mintz and Arakawa, 1963; Mintz, 1965; Leith, 1965; Smagorinsky et al, 1965; Manabe et al, 1965 and 1970) made further attempts to simulate the general circulation by using more and more sophisticated models. Very few attempts, however, have been made to simulate weather systems of the scale of the Indian summer monsoon.

4.2 Methodology of Simulation

A simplified model is formulated in which only a zonally averaged motion has been taken into account in

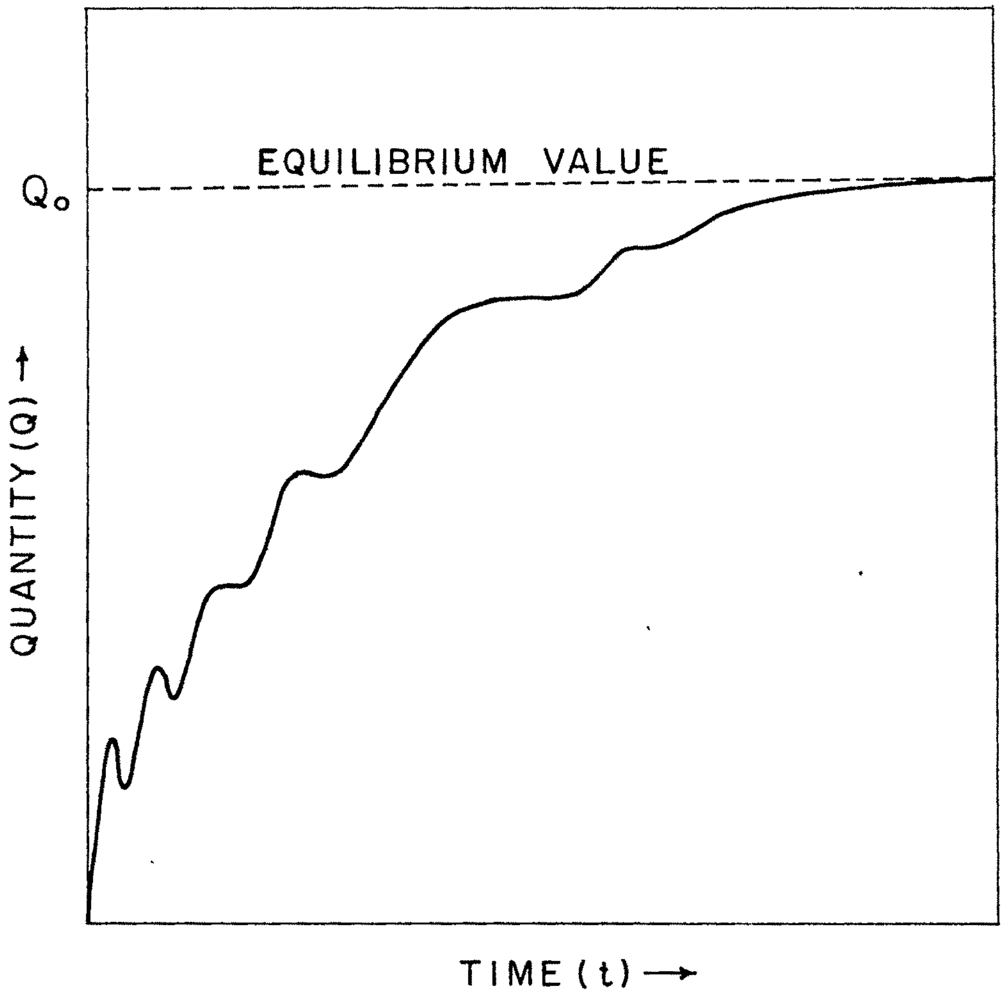

Figure 4.1.1 Schematic representation of variation of any quantity (Q) with respect to time having an asymptotic solution.

the two dimensional vertical plane along 80°E. No disturbance is superimposed upon the zonal current. To start with, the region extending from equator upto north pole has been considered for computational purposes. In the horizontal, 18 grid-points at 5 degree latitude interval have been used as shown in Figure 4.3.1 A. The grid point "1" is located at half the grid distance outside the equator and the grid-point "20" is similarly located outside the north pole. In latter experiments, however, the region has been shifted southward so that the southern boundary (grid-point "1") coincides with 37.5°S and the northern boundary (grid-point "20") at 57.5°N. In the vertical, the sigma (σ) system of coordinates has been used to facilitate inclusion of topography. The free atmosphere has been divided into eight levels. The top of the turbulence layer coincides with level "$8\frac{1}{2}$" and the ground is represented by level "9" (Figure 4.2.1 B). For details see Appendix A. The latitudinal dependence of sigma-levels is shown in Figure 4.2.2. For convenience, the northern boundary of the Indian Ocean is fixed at 15°N. The region corresponding to the top of the Himalayas coincides with latitude 32.5°N.

The role of radiation has been considered in detail. The radiational heating due to both short and long wave has been computed from the available

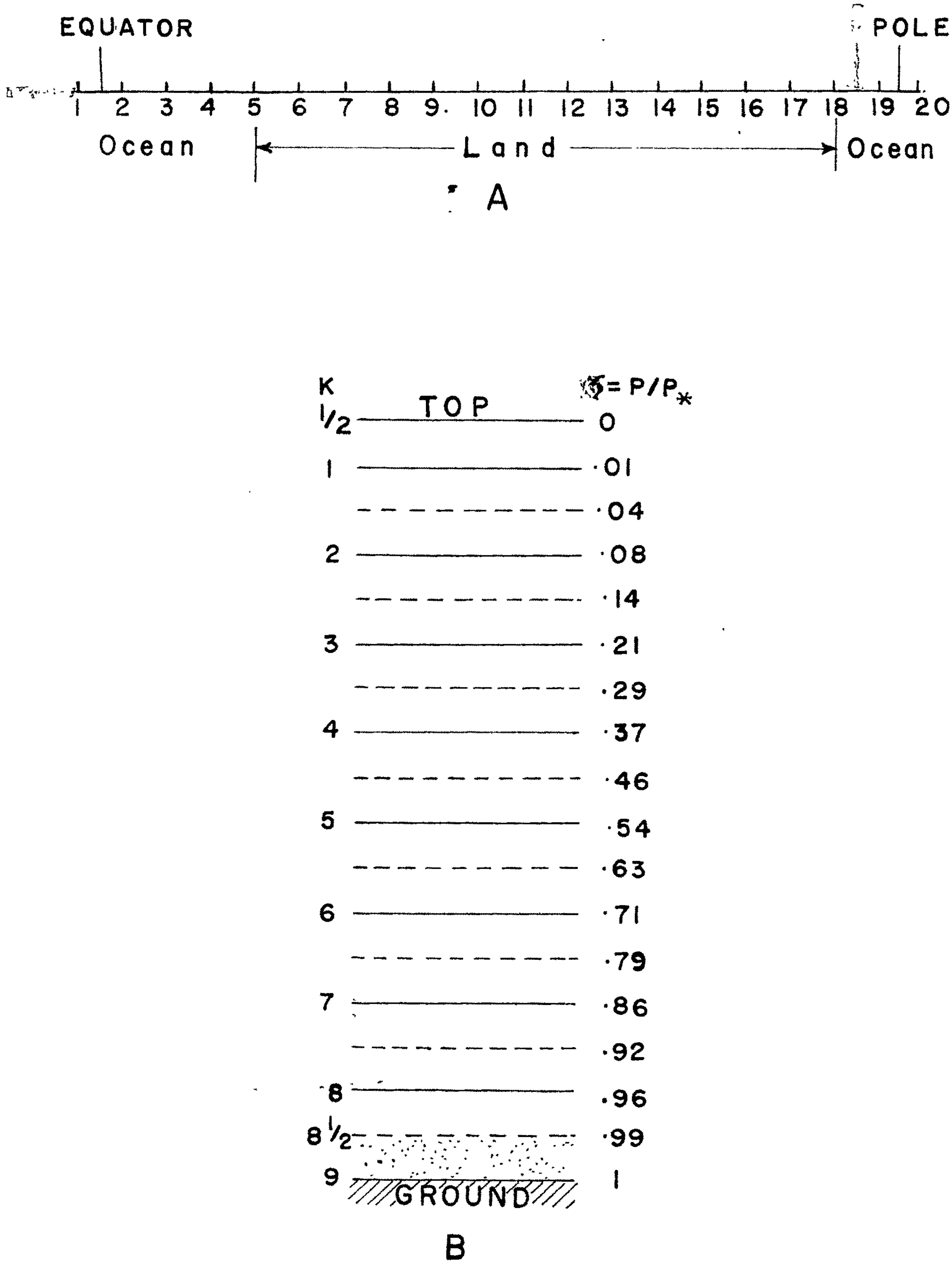

Figure 4.2.1 (A) Horizontal grid in the north-south direction. The grid interval is 5 degree latitude. (B) Various sigma-levels in the vertical from the ground upto the top of the atmosphere.

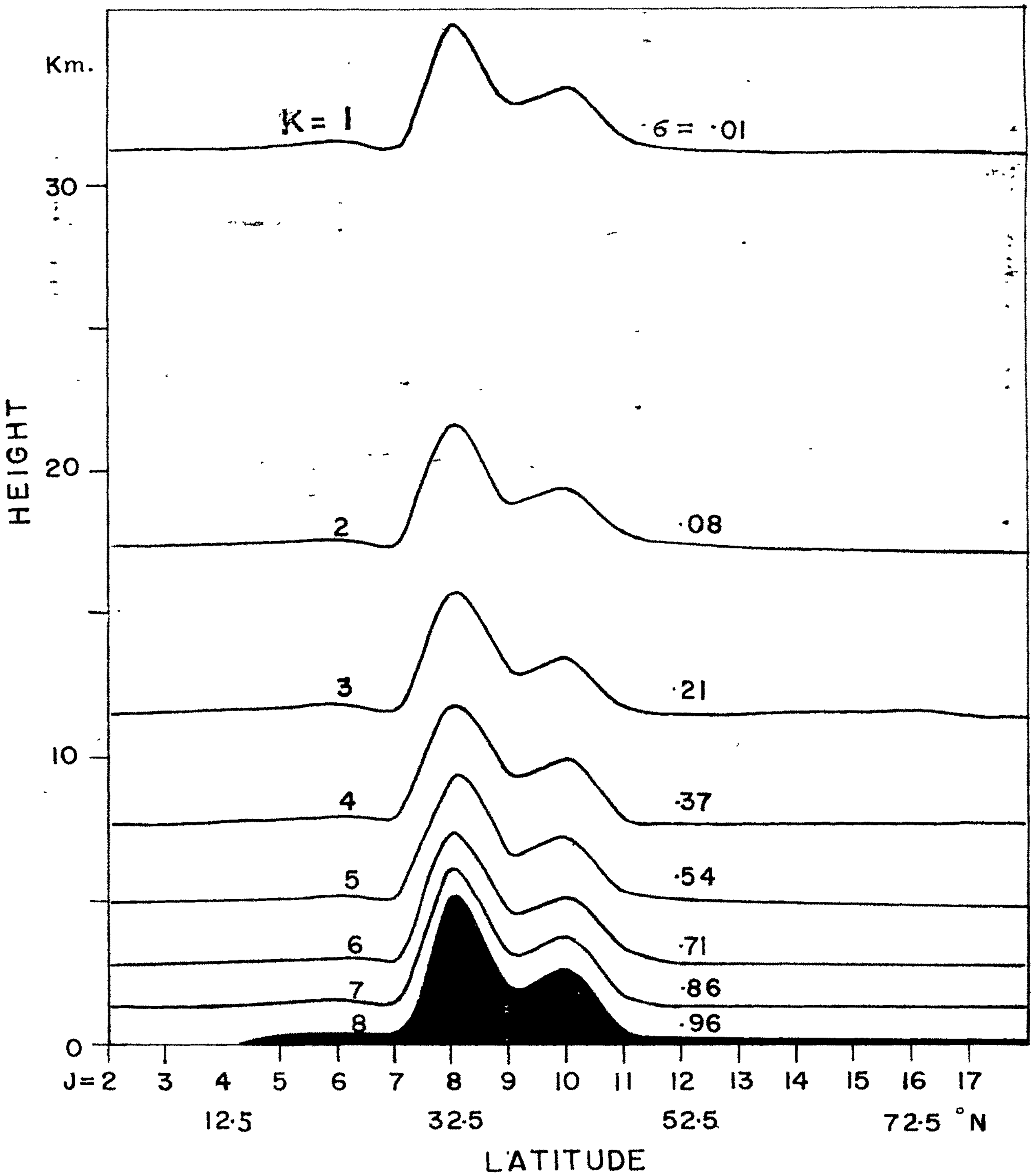

Figure 4.2.2 Latitudinal variation of the height of the sigma-level.

distributions of water vapour, carbon dioxide and ozone for July month which is typical of the monsoon season. Albedo at the earth's surface has been determined from the Smithsonian Tables (Table No. 154) by considering the cloud amount, precipitation and surface conditions during the monsoon season. Assuming the heat capacity of the ocean to be infinite, the sea surface temperature has been kept constant. Over the continent, the surface tempera--ture has been determined as the balance between the various thermal components i.e. long wave radiation, solar radia--tion, and sensible and latent heat fluxes.

Condensation due to meridional circulation and convection has been considered. Convective effect is taken into account such that temperature in any layer is adjusted to dry (wet) adiabatic lapse rate whenever the temperature distribution in that layer exceeds dry (wet) adiabatic lapse rate for humidity less (more) than 100 per cent. Prandtle's turbulence theory which takes into account only forced convection has been used in the case of the turbulence layer. The values of the roughness parameter considered for sea, land, and mountain have been arbitrarily chosen as 0.1 cm, 1.0 cm, and 10 cm respectively.

The experiment has been performed for the follow--ing sets of conditions : (1) with moisture and with the Himalayas (wet model with the Himalayas), (2) without moisture and with the Himalayas (dry model with the

Himalayas), (3) without moisture and without the Himalayas (dry model without the Himalayas), and (4) with moisture and without the Himalayas (wet model without the Himalayas). Experiment (3) has been subdivided with respect to two given sea surface temperatures, namely, 300°K and 290°K. Also, experiment (4) has been subdivided according to the two different surface mixing ratio values considered, namely, 80 percent and 40 percent of saturation mixing ratio at the surface, and also according to the assumed condition that condensation occurs at 80 percent relative humidity.

Using finite different scheme, which is designed to conserve energy, the solution is obtained by marching process referred to earlier. Initially the atmosphere is assumed to be at rest ($u = v = w = o$) and the only force considered is that due to radiation. The time interval of integration is taken as 10 minutes and hence the integration time of one day corresponds to 144 time steps. The marching process is continued until the equilibrium condition is reached in which case the rates of change of u, v and T with respect to time are sufficiently small (as seen from Figure 4.1.1). In practice, equilibrium is considered to have been reached when the difference between the daily mean temperatures simulated of two consecutive days was less than 0.1°C.

4.3 Prognostic Equations

The parameters to be predicted are the velocity components (u, v), the temperature (T), and the water vapour mixing ratio (r). The equations for the zonally averaged motion in spherical coordinates and in terms of σ, as the vertical coordinate, may be written as

$$\frac{\partial p_* u}{\partial t} = -\frac{\partial p_* u v \cos\varphi}{a\cos\varphi\,\partial\varphi} - \frac{\partial p_* u \dot{\sigma}}{\partial\sigma} + \left(f + \frac{\tan\varphi}{a}u\right)p_* v + p_* F_\lambda \tag{4.3.1}$$

$$\frac{\partial p_* v}{\partial t} = -\frac{\partial p_* v^2 \cos\varphi}{a\cos\varphi\,\partial\varphi} - \frac{\partial p_* v \dot{\sigma}}{\partial\sigma} + \left(f + \frac{\tan\varphi}{a}u\right)p_* u + \sigma\frac{\partial\bar{\Phi}}{\partial\sigma}\frac{\partial p_*}{a\,\partial\varphi} - p_*\frac{\partial\bar{\Phi}}{a\,\partial\varphi} + p_* F_\varphi \tag{4.3.2}$$

$$\frac{\partial p_* T}{\partial t} = -\frac{\partial p_* T v \cos\varphi}{a\cos\varphi\,\partial\varphi} - \frac{\partial p_* T\dot{\sigma}}{\partial\sigma} - \frac{\omega}{c_p}\frac{\partial\bar{\Phi}}{\partial\sigma} + \frac{1}{c_p}p_*\dot{q} + p_* F_T \tag{4.3.3}$$

$$\frac{\partial p_* r}{\partial t} = -\frac{\partial p_* r v \cos\varphi}{a\cos\varphi\,\partial\varphi} - \frac{\partial p_* r\dot{\sigma}}{\partial\sigma} - p_* C + p_* F_r \tag{4.3.4}$$

The continuity equation may be written as

$$\frac{\partial p_*}{\partial t} = -\frac{\partial p_* v\cos\varphi}{a\cos\varphi\,\partial\varphi} - \frac{\partial p_*\dot{\sigma}}{\partial\sigma} \tag{4.3.5}$$

The hydrostatic balance may be expressed as

$$\frac{\partial \Phi}{\partial \sigma} = -\frac{RT}{\sigma} \qquad (4.3.6)$$

The vertical velocity ω may be written as

$$\omega = p_* \overset{\circ}{\sigma} + \sigma \left(\frac{\partial p_*}{\partial t} + v \frac{\partial p_*}{a \partial \varphi} \right) \qquad (4.3.7)$$

All the variables appearing in the above equations are functions of φ, σ, and t. The notations of the constants and variables used are as follows :

p_* Pressure at the earth's surface

p Pressure at any level

φ Latitude

σ p/p_*

$\overset{\circ}{\sigma}$ $d\sigma/dt$

u Zonal wind velocity

v Meridional wind velocity

T Temperature

r Mixing ratio of water vapour

Φ Geopotential height of σ- surface

ω dp/dt

$\overset{\circ}{q}$ Rate of non-adiabatic heating (radiation and condensation)

F_λ Frictional effect in the zonal direction

F_φ Frictional effect in the meridional direction

F_T Frictional effect due to diffusion of heat

F_r Frictional effect due to diffusion of water vapour

C Amount of condensation

f Coriolis parameter

a Radius of the earth

c_p Specific heat of air at constant pressure

R Universal gas constant

4.3.1 Friction

The last terms each on the right of equations (4.3.1) to (4.3.4) represent the effect of friction due to Reynold's stresses (equations 4.3.1 and 4.3.2) and due to eddy diffusion of heat and water vapour (equations 4.3.3 and 4.3.4). These terms are elborated in detail in Appendix B.

4.3.2 Radiation

Radiation is considered to be the primary force to drive the monsoon circulation. Its contribution ($\mathring{q}$) appears in the fourth term on the right of equation (4.3.3). The experiment starts with a completely calm and dry atmosphere with the same vertical temperature distribu--tion as the U.S.standard atmosphere (U.S.Air Force, (1962), so that, there is no horizontal gradient of tempe--rature and geopotential along any isobaric level at the initial time step. However, this initial vertical tempera--ture distribution is quickly disturbed as inequality sets in the radiational heating. In order to compensate for the heat contrast, which is developed, motion will start gradually ultimately leading to the monsoon circulation.

The treatment for computing the absorption of solar and long wave radiation by water vapour, carbon dioxide, and ozone has been described in detail in Appendix C.

4.3.3 Convection and condensation

The effect of convection is incorporated in the model indirectly by adopting a simplified process (Manabe, et al, 1965) of dry and wet convective adjustments of temperature and water vapour as a substitute for the actual convective process. The vertical distribution of tempera--ture in any layer of a column is adjusted to dry (wet) adiabatic lapse rate whenever the distribution of tempera--ture exceeds dry (wet) adiabatic lapse rate for humidity less (more) than 100 per cent. In making the adjustment it is assumed that the kinetic energy created by convection is converted into heat instantaneously so that the total potential energy remains invariant. In wet convective adjustment it is assumed that all the water vapour which is condensed precipitates instantaneously. The temperature is adjusted corresponding to the amount of latent heat which is released in the process of condensation.

Condensation which occurs due to non-convective processes is also taken into account. In any layer of air column where the relative humidity excees 100 per cent with its temperature lapse rate less than wet adiabatic lapse rate, the vertical distribution of relative humidity is adjusted to 100 per cent. As in the case of wet convective adjustment, the excess of water vapour which is condensed is assumed to precipitate instantaneously and the temperature is adjusted corresponding to the amount of latent heat which is released in the process of condensation (For details see Appendix C).

4.3.4 Boundary Condition

The vertical boundary conditions are such that at the top and the bottom of the atmosphere, the vertical σ-velocity is zero, i.e.

$$\overset{\circ}{\sigma} = 0 \ , \text{ at } \sigma = 0, 1 \qquad (4.3.8)$$

The lateral boundary conditions are introduced such that at the equator and at the pole, no transport of momentum, heat and moisture is allowed to take place i.e.

$v = 0$ at the equator and the pole (4.3.9)

In order to exclude the possibility of the generation of gravity waves at the lateral boundaries, the following condition is used.

$u = 0$ at the equator and the pole (4.3.10)

At the top of the atmosphere, the downward long wave radiation is assumed to be zero. The value for solar constant considered is 2 ly $\min^{-1}$.

At the earth's surface, the temperature is determined such that it satisfies the requirement of the heat balance at the earth's surface. The balance equation may be written as

$$S_* + (DLR)_* = \sigma T_*^4 - c_p \left(\gamma_*^z + \frac{L}{c_p} \mu_*^z \right) \qquad (4.3.11)$$

In the above, S_* and $(DLR)_*$ are the net downward solar radiation and the downward long wave radiation respectively at the earth's surface. σ is the Stefan-Boltzman constant. $c_p \gamma_*^z$ and $L \mu_*^z$ represent the upward sensible and latent heat exchange respectively at the earth-atmosphere interface which are ultimately functions of surface wind and temperature gradient across the earth-atmosphere interface (for details see Appendix B).

4.4 Basic Data

Water vapour : The mixing ratio of water vapour has been determined by using Monthly Climatic Data for the World for July 1964-65 published by ESSA of United States. Analysis of the mixing ratio at standard isobaric levels has been made for the region from 0 to 90° N and from 70° to 100° E and the values were read at each grid point along 80° E. These were further plotted individually as height-temperature profiles. Mixing ratio above 500 mb was extrapolated untill a line of constant frost point of 190° K is reached. Thereafter, the mixing ratio was assumed as stated in Section 2.3, to follow constant frost point of 190°K irrespective of latitude upto a height of 30 km, as considered by Manabe and Moller (1961). Above 30 km, a constant mixing ratio line has been followed.

At the earth's surface, the mixing ratio of water vapour has been determined by using the relation

$$r_* = \beta r_s (T_*) \tag{4.4.1}$$

where r_* is the mixing ratio at the earth's surface. β is a constant arbitrarily fixed and $r_s(T_*)$ is the saturation mixing ratio at the earth's surface temperature T_*. β is considered to be unity for the sea surface. It is assumed to be 0.8 for the land and 0.6 for the mountain. The distribution of water vapour, thus determined, is presented in Figure 4.4.1.

Carbon dioxide : The mixing ratio has been assumed to be constant at 0.456 (gm/kgm) for all the levels and for all the latitudes.

Ozone: The mixing ratio has been determined on the basis of the ozone Data of the World published by the meteorological service of Canada and on the basis of the cross-sections earlier published by (1) Ramanathan and Kulkarni (1960), and (ii) Murgatroyd

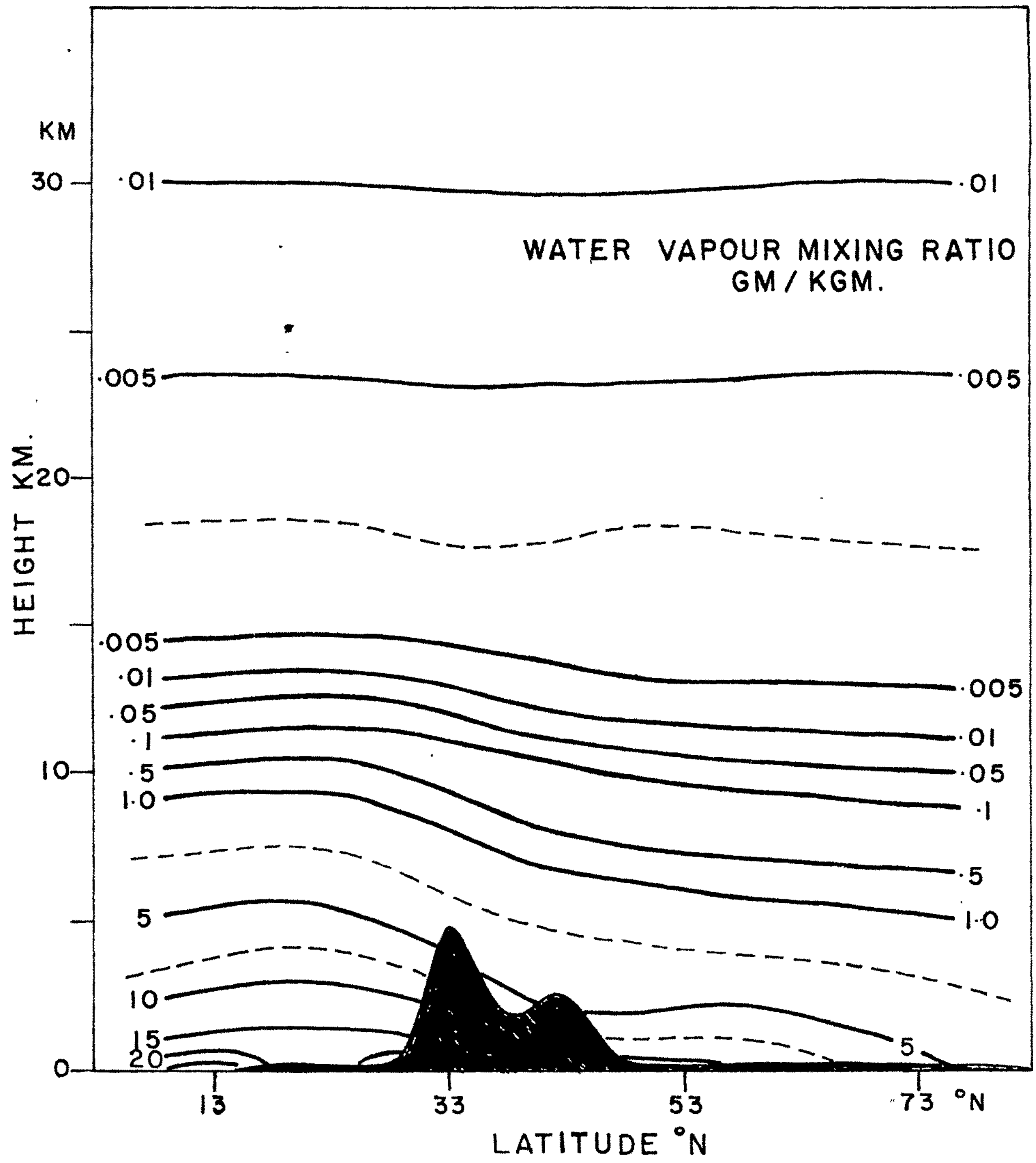

Figure 4.4.1 Distribution of water vapour (gm/kgm) as a function of latitude and height.

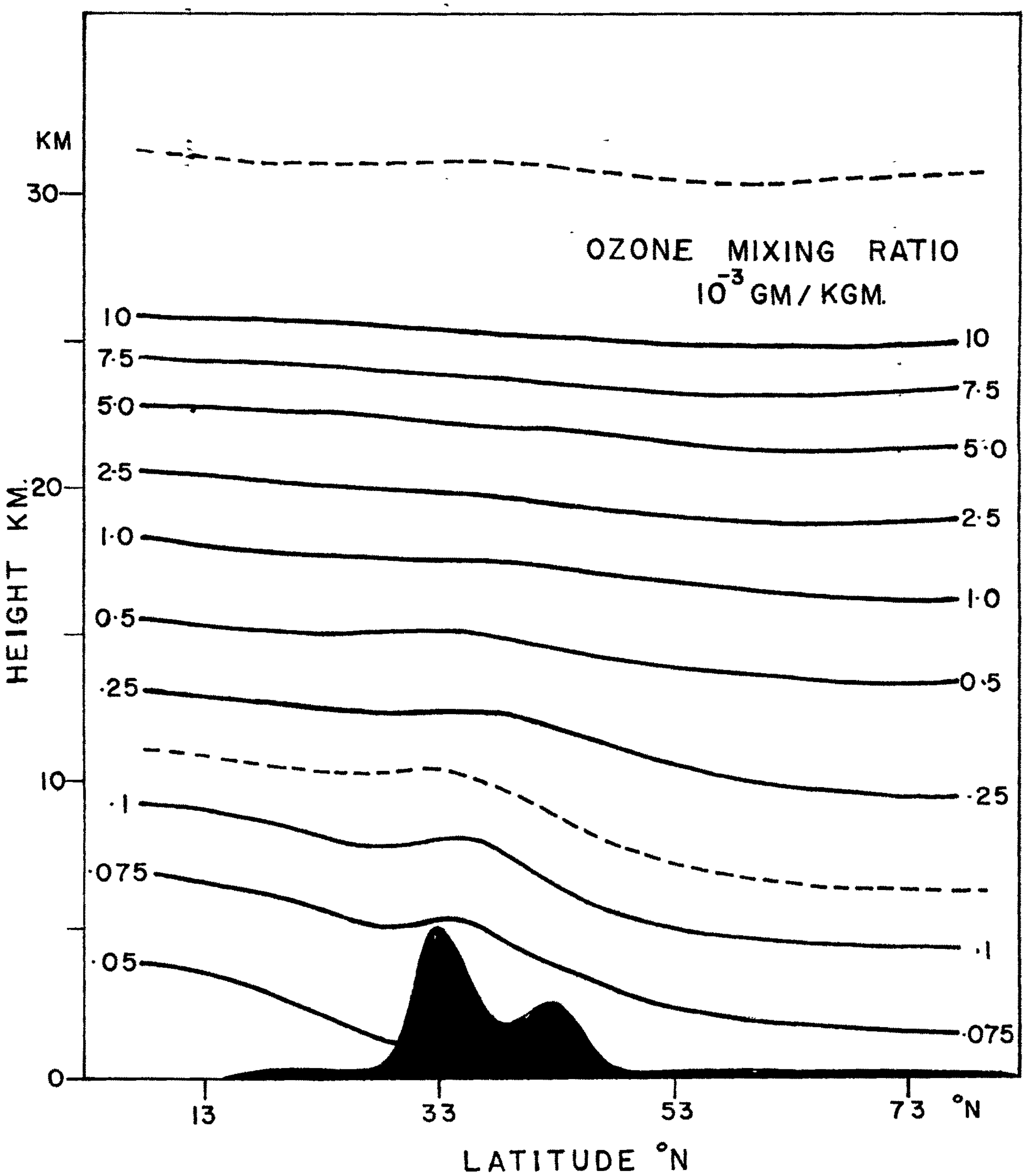

Figure 4.4.2 Distribution of ozone (10^{-3} gm/kgm) as a function of latitude and height.

(1964). In Figure 4.4.2, is shown the ozone distribution with respect to height and latitude.

Albedo: The values of surface albedo as given by the Smithsonian Tables (Table No. 154) for different surface conditions have been adopted.

Cloud : The cloud amount has been determined from the Daily Weather Map with Synoptic Data Tabulation of Japan Meteorological Anency and the Daily Series, Northern Hemispheric Data Tabulations of the U.S. Weather Bureau for July 1964-1965.

Absroptivity and emissivity : The values of mean slab absorptivity and emissivity for water vapour, carbon dioxide and ozone and also the values of absorption of solar radiation by these gases, as given by Manabe and Moller (1961), have been used.

4.5 Results and Discussion

As the monsoon activity is limited to the South of the Himalayas, results are presented for the region from equator to 40°N.

4.5.1 Wet model with the Himalayas

Evaporation at the earth's surface (corresponding to $\beta = 0.8$ in equation 4.4.1) and condensation in the free atmosphere have been considered. Figure 4.5.1 shows

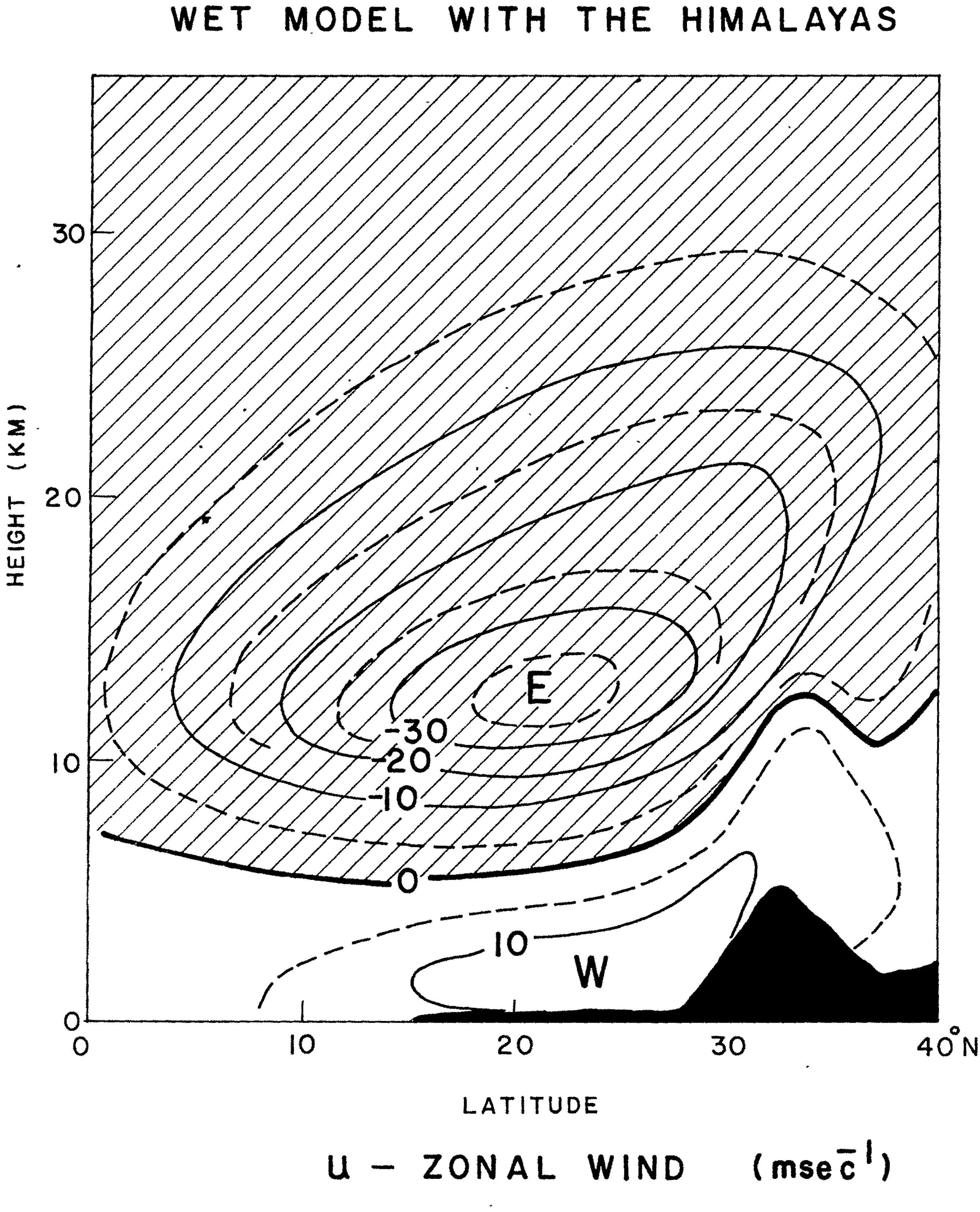

Figure 4.5.1 Vertical cross section of simulated zonal wind ($m\ sec^{-1}$) along 80°E for wet model with the Himalayas. Easterly (E) regime is hatched.

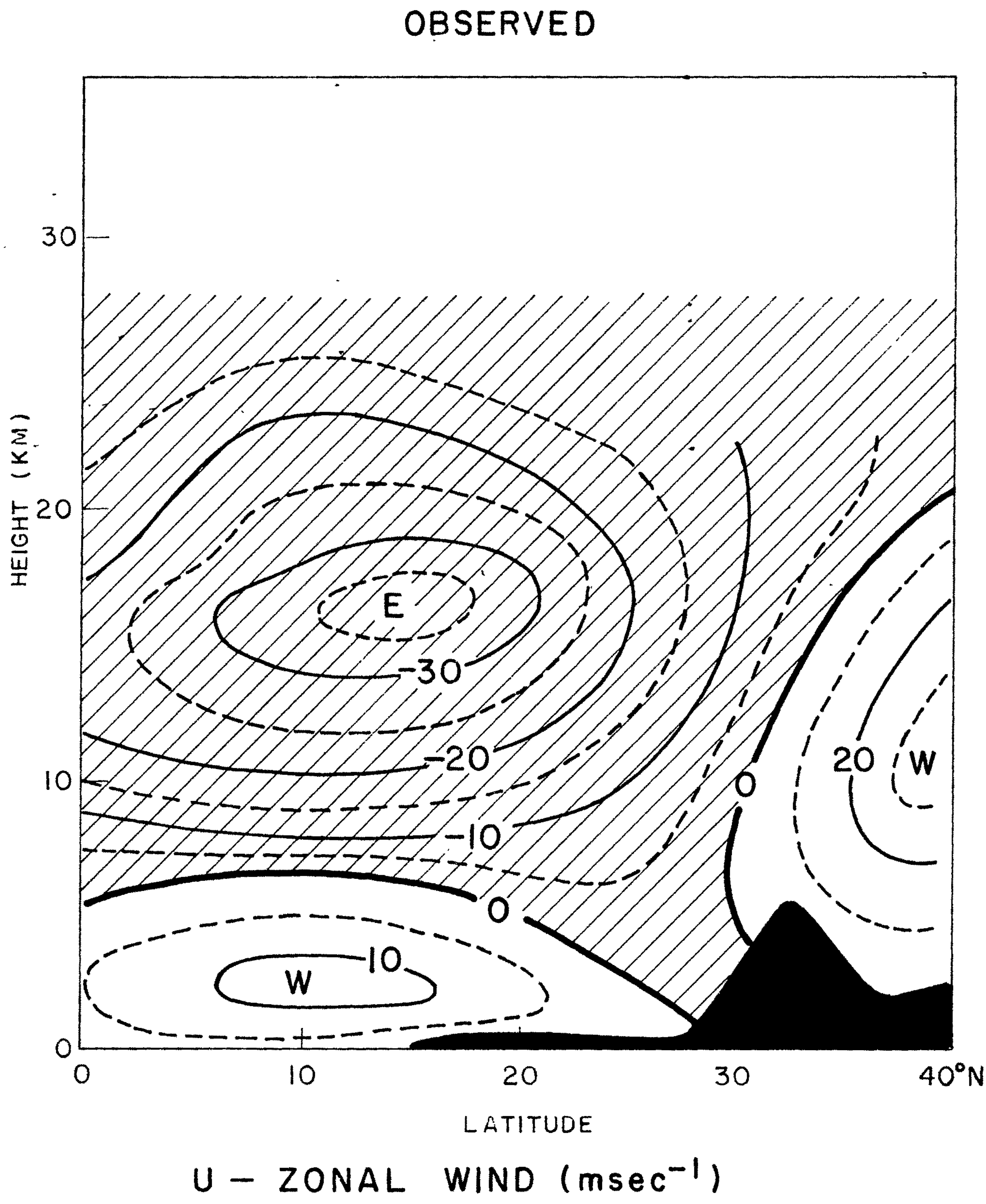

Figure 4.5.2 Vertical cross section of observed zonal wind (m sec^{-1}) along 80 E. Easterly (E) regime is hatched.

the distribution of simulated zonal wind with respect to height and latitude. The essential features which are indicated are the existence of (1) Tropical Easterly Jet (TEJ) at 12 km with core speed of 36 m sec^{-1} at 20°N, and (2) low-level westerly of more than 10 m sec^{-1} extending from south of the Himalayas to 17°N. The depth of the westerlies, which is about 7 km at the equator, shows a slight decrease northward upto 17° N but increases rapidly thereafter reaching 10 km at 35°N. The overlying easterlies extend upto the maximum level considered (35 km).

Figure 4.5.2 shows the vertical cross section of the observed mean zonal wind during July from equator to 40°N which is prepared from the analyses presented in Section 2.3 (Figures 2.4.1 A and 2.4.2). The analysis above 100 mb is based on the available data for 50 and 30 mb, being supplemented by the results of Flohn (1964) and Koteswaram (1969). Comparision of Figures 4.5.1 and 4.5.2 points out that there is agreement between the simulated and the observed wind pattern in so far as the main features are concerned, i.e. the upper level easterlies with TEJ and the low-level westerly flow to the south of the Himalayas. However, the increasing tendency in the depth of the westerly with latitude northward from 17°N indicated by the simulated pattern is absent

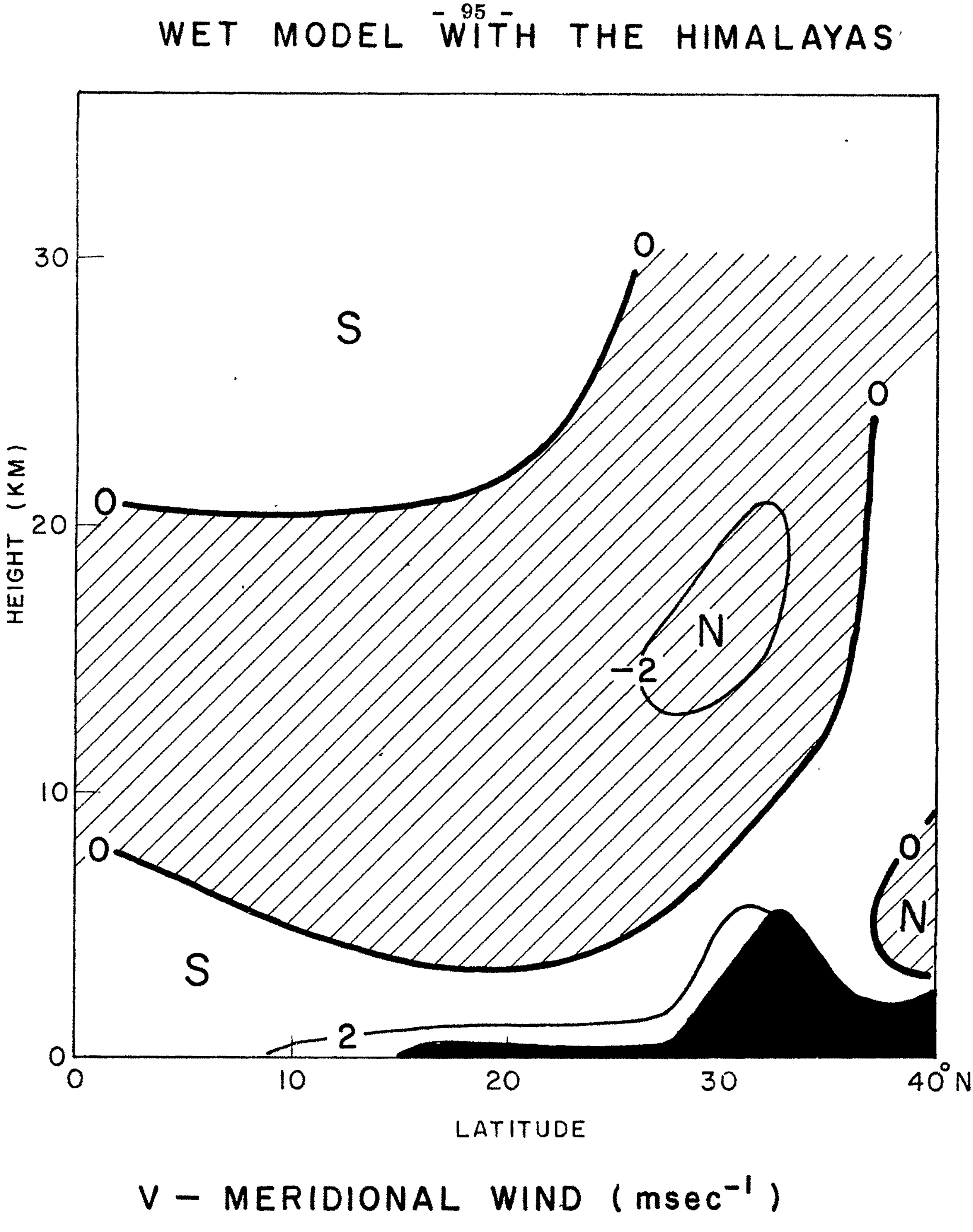

Figure 4.5.3 Vertical cross section of simulated meridional wind (m sec^{-1}) along 80°E for wet model with the Himalayas. Northerly (N) regime is hatched.

OBSERVED

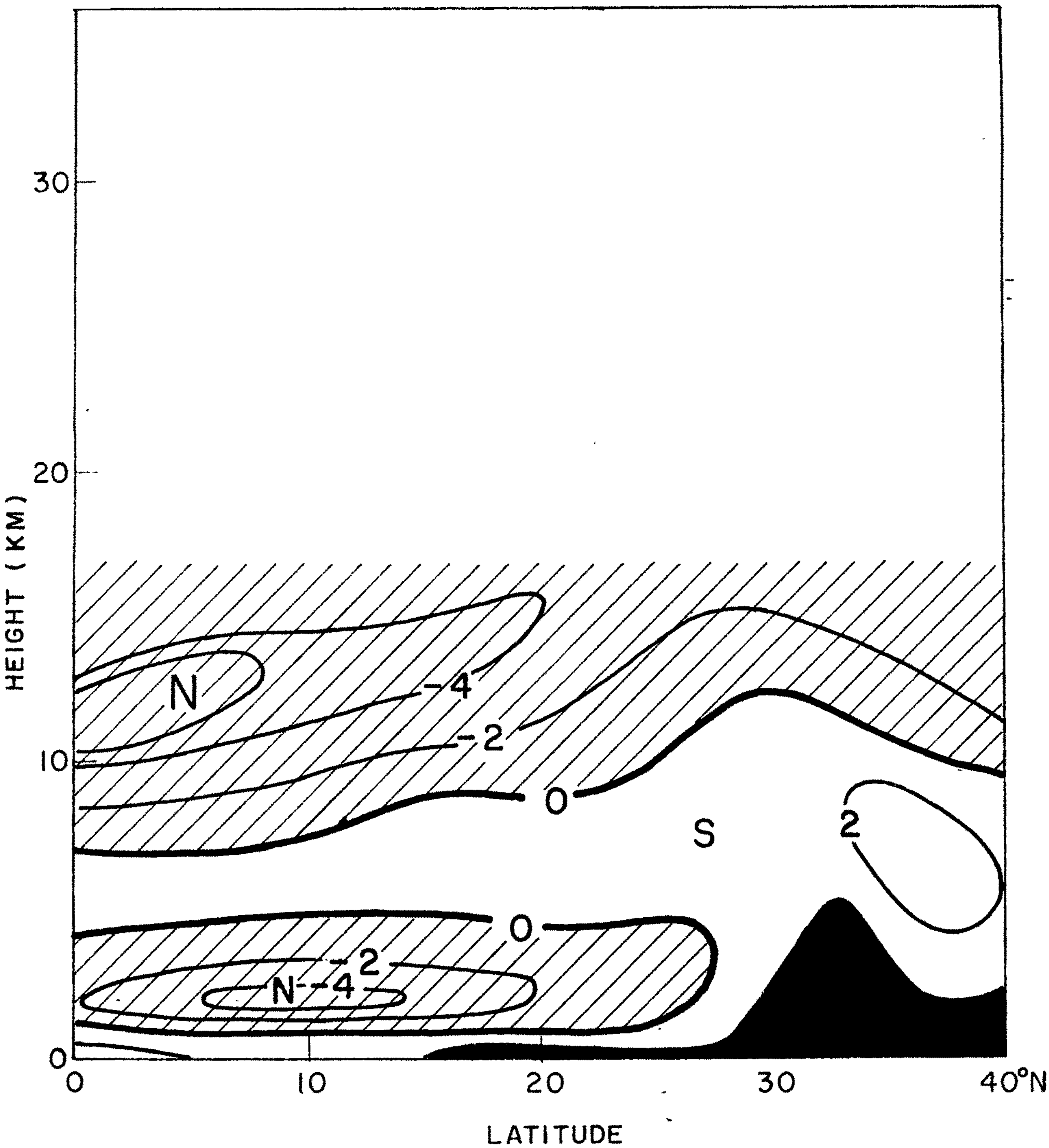

V — MERIDIONAL WIND ($msec^{-1}$)

Figure 4.5.4 Vertical cross section of observed meridional wind ($m\ sec^{-1}$) along 80°E. Northerly (N) regime is hatched.

in the observed wind pattern. Instead, its depth, in the observed pattern, decreases progressively with latitude from equator to 30°N.

The vertical cross section of the simulated meridional wind is shown in Figure 4.5.3. In the lower troposphere, the wind is southerly with a maximum speed of 4.3 m sec^{-1} near the surface. In the upper troposphere and lower stratosphere (upto 20 km) northerly wind with a maximum speed of 2 m sec^{-1} prevails. The northerly extends even into the middle stratosphere (upto 30 km). Thus, the simulated pattern south of the Himalayas exhibits the features of direct circula--tion cell as characterised by southerlies below and northerlies aloft. This circulation has been identified as the monsoon cell.

The vertical cross section of the observed meridional component of wind is shown in Figure 4.5.4 which has been prepared from the analyses presented in section 2.3 (Figures 2.4.1 B and 2.4.3). Southerly is observed near the surface and in the middle troposphere and northerly in the lower and in the upper troposphere. Comparision with Figure 4.5.3 shows that the simulated northerly wind is weaker than the observed. Also, the northerly which is observed in the middle troposphere is absent in the simulated wind field.

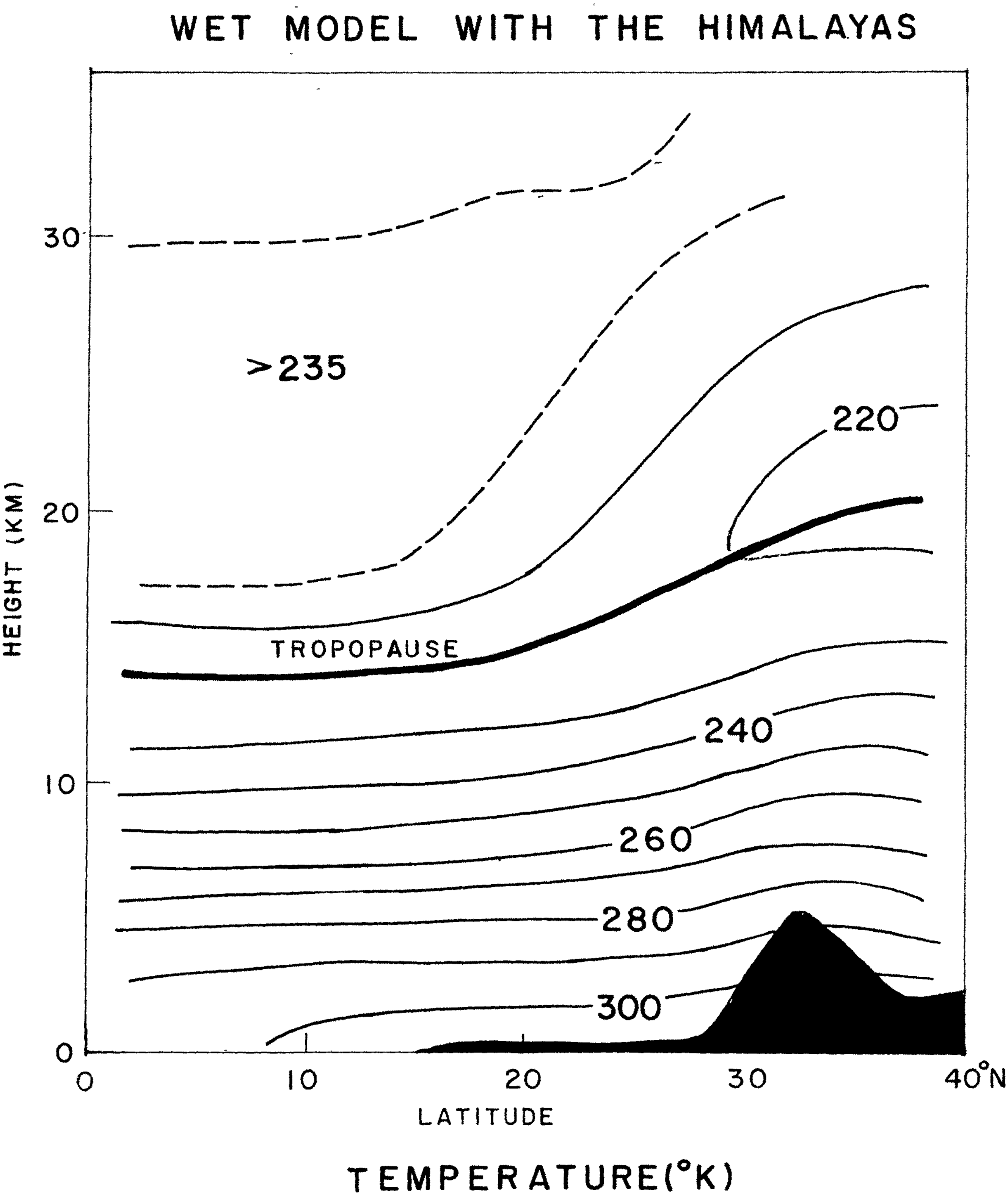

Figure 4.5.5 Vertical cross section of simulated temperature (°K) along 80°E for wet model with the Himalayas. Solid line represents tropopause.

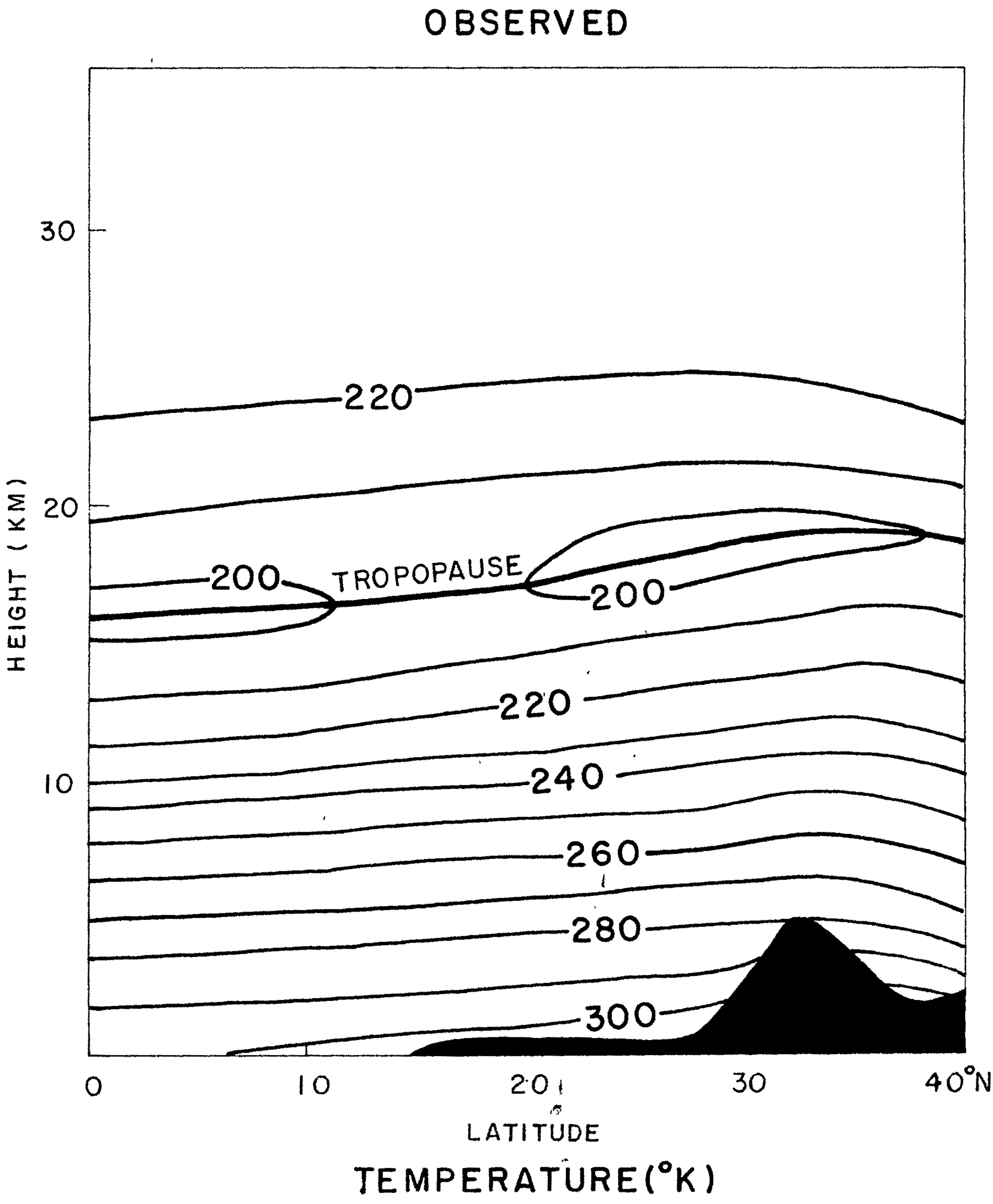

Figure 4.5.6 Vertical cross section of observed temperature (°K) along 80°E. Solid line represents tropopause.

In figure 4.5.5 is shown the distribution of the simulated temperature with respect to height and latitude. The air in the region above the Himalayas is warmer than that over the equatorial regions considered at the same level. The higher temperatures indicated northward are consistent with the strong and upward increasing tropospheric easterlies noticed over India (Flohn 1960; Koteswaram, 1960).

The other conspicuous features brought out by the simulated temperature field are (i) the temperature at the tropopause level is minimum over the Himalayas, and (ii) the height of the tropopause increases with latitude.

For comparison a vertical cross section of mean July temperature field has been presented from the temperature analyses of section 2.3 (Figures 2.3.1 and 2.4.4). The results which are shown in Figure 4.5.6 are in agreement with those obtained by simulation. However, these are at variance with the global mean temperature cross section given by London et al (1956) for July. The findings, therefore, point out that the conventional global features available in the literature are not applicable for the Indian longitudes where the presence of the Himalayas exercise considerable influence on the monsoon circulation.

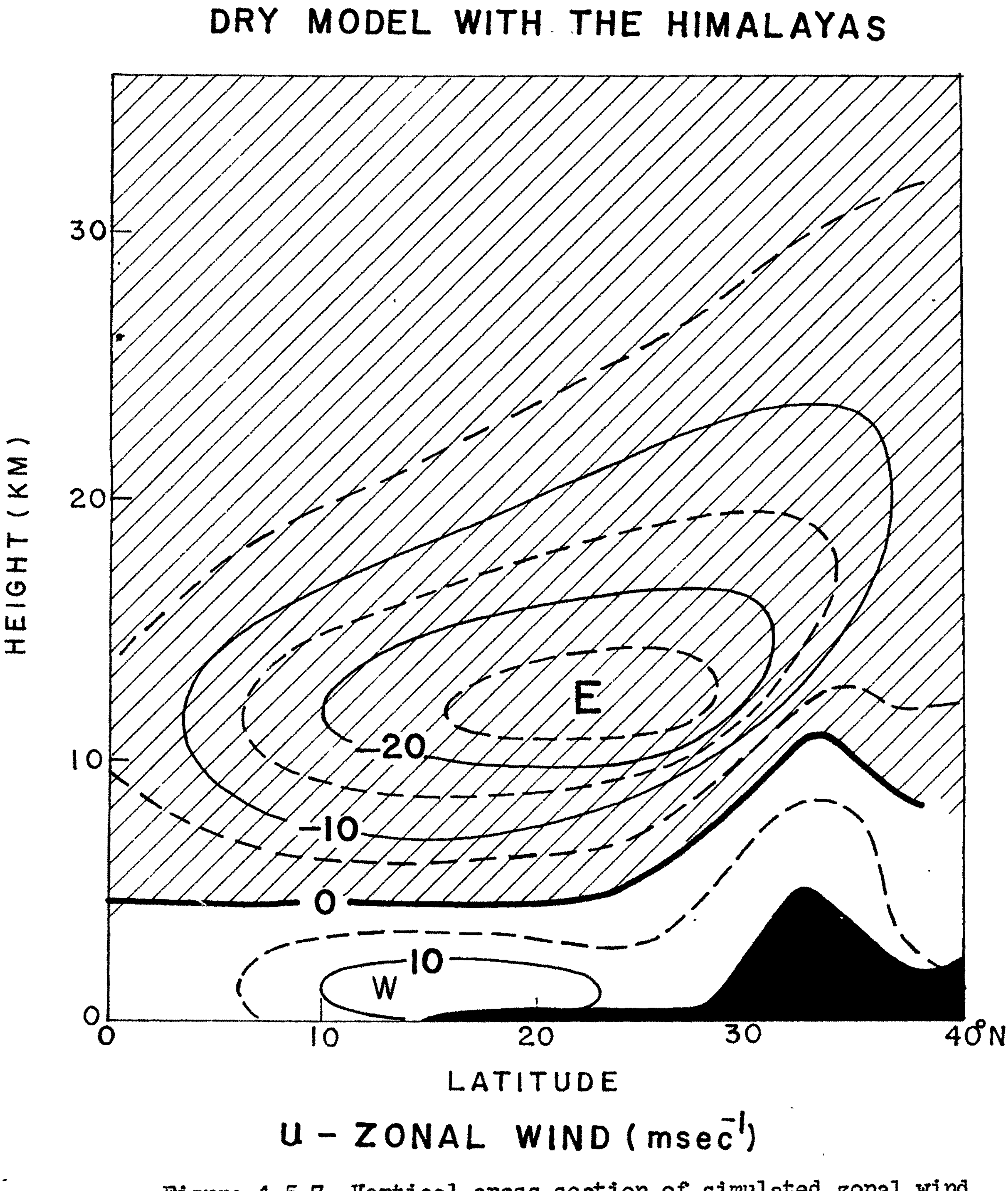

Figure 4.5.7 Vertical cross section of simulated zonal wind (m sec^{-1}) along 80°E for dry model with the Himalayas. Easterly (E) regime is hatched.

4.5.2 Dry model with the Himalayas

As the atmosphere is assumed to be dry there is no evaporation at the earth's surface and no condensation in the atmosphere. The results are shown in Figure 4.5.7 in which the zonal wind is plotted with respect to height and latitude. Comparison with Figure 4.5.1 (wet model with the Himalayas) shows that there is no pronounced difference between the configurations of the two wind fields. The winds obtained by the dry model are only slightly weaker than those obtained by the wet model. The core speed of the easterly jet decreases from 30 m sec^{-1} in the wet model (Figure 4.5.1) to 25 m sec^{-1} in the dry model (Figure 4.5.7). The low level westerly also decreases from 14 m sec^{-1} to 12 m sec^{-1}. The results, therefore, point out that moisture is not the essential criterion for the generation of the monsoon circulation.

4.5.3 Dry model without the Himalayas

The atmosphere is assumed to be dry as in the earlier experiment. In addition, the presence of the Himalayas is not taken into account. The experiment has been performed, as already stated, for two sea surface temperatures, namely 300° K and 290° K.

(a) Sea surface temperature at 300° K : The vertical

DRY MODEL WITHOUT THE HIMALAYAS
(SEA SURFACE TEMP. 300°K)

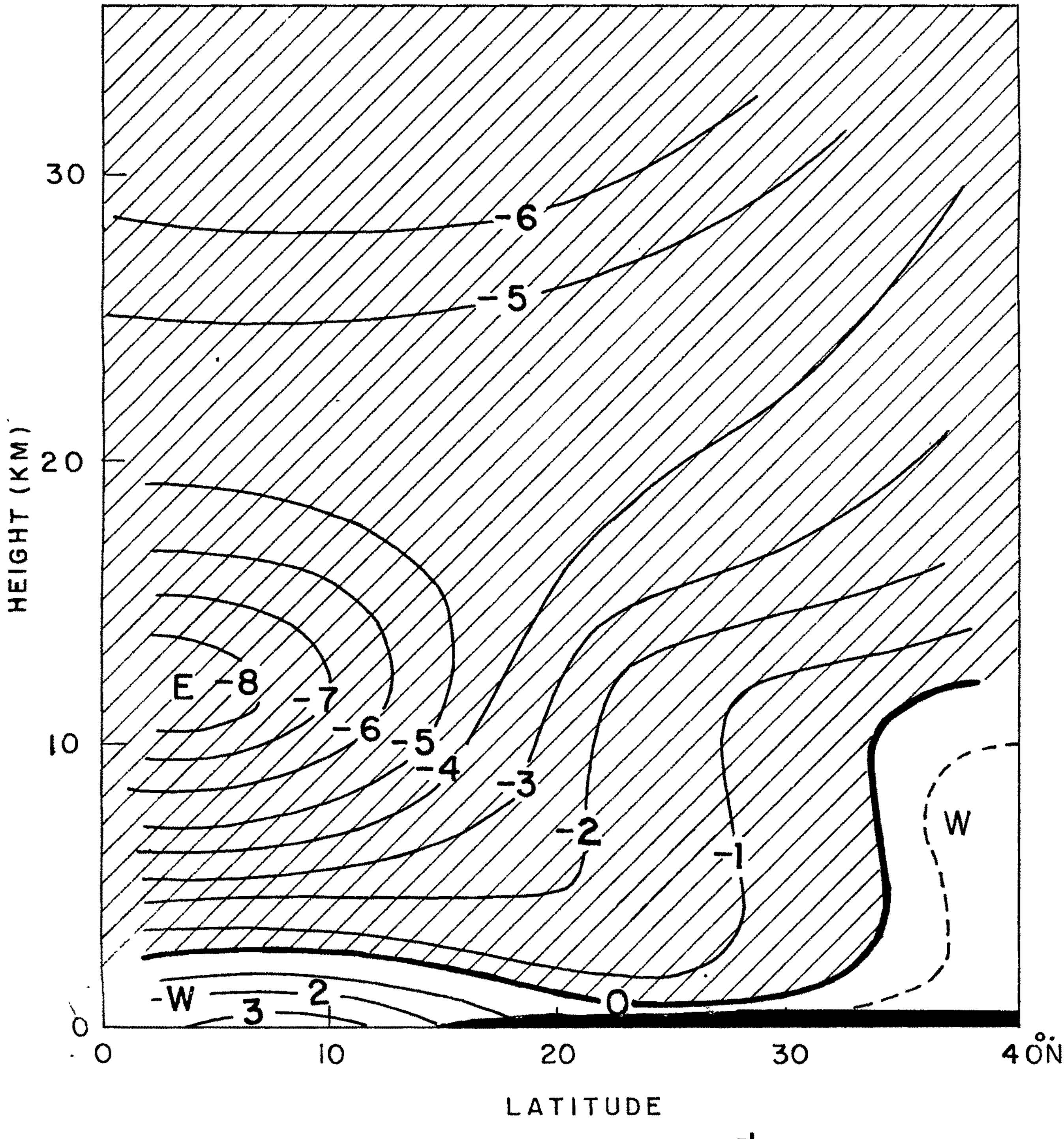

u - ZONAL WIND (m sec^{-1})

Figure 4.5.8 Vertical cross section of simulated zonal wind (m sec^{-1}) along 80°E for dry model without the Himalayas with sea surface temperature fixed at 300°K. Easterly (E) regime is hatched.

cross section of the zonal wind component simulated is shown in Figure 4.5.8. In the region to the south of 25°N, the westerly current prevails in the lower levels while the easterly flow overlies aloft, and the height of the boundary between the westerly and the easterly decreases northward in the manner as observed. It may have to be emphasised, therefore, that one of the important characteristic features of the monsoon circulation i.e. the westerlies in the lower troposphere capped by the easterlies aloft, has been qualitatively simulated even by using this very simplified model, namely, dry model without the Himalayas. But, the circulation indicated is weak, especially in the upper troposphere. Comparing Figure 4.5.8 (simulated pattern) with Figure 4.5.2 (observed pattern), it is seen that in place of the tropical easterly Jet (TEJ) with core speed of 30 m sec^{-1}, there has been a very weak easterly simulated with core speed of only 8 m sec^{-1}. Similarly, the intensity of the westerly simulated is less than the observed by a factor of three. The depth of the westerly generated is also 2 to 3 times smaller than the observed.

(b) Sea surface temperature at 290° K : The vertical cross section of zonal wind obtained is illustrated in Figure 4.5.9. Comparison of features as seen in Figures 4.5.8 (for sea surface temperature at 300° K) and

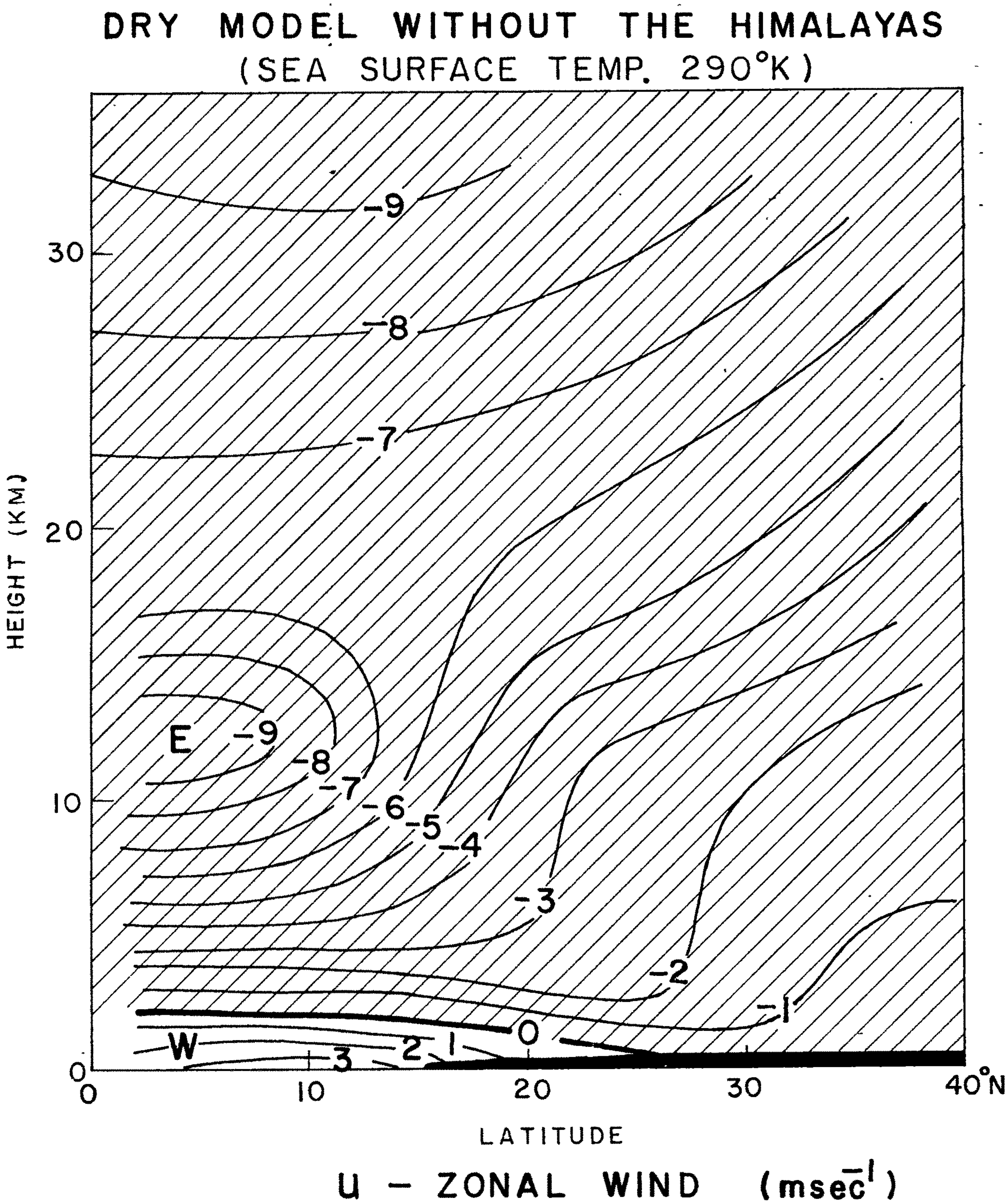

Figure 4.5.9 Vertical cross section of simulated zonal wind ($m\ sec^{-1}$) along 80°E for dry model without the Himalayas with sea surface temperature fixed at 290°K. Easterly (E) regime is hatched.

4.5.9 points out that there is practically no difference in the pattern obtained either with respect to the depth and the extent of the westerlies or the strength and the location of the easterlies. The circulation with sea surface temperature at 290° K is slightly stronger (easterly core speed of 9 m sec^{-1}) than that with sea surface temperature at 300° K (easterly core speed of 8 m sec^{-1}). The findings clearly being out that the surface temperature of the Indian Ocean is not a dominant factor in determing the intensity of the - monsoon circulation.

The ocean-continent temperature contrast obtained in the foregoing wet and dry model experiments (Sections 4.5.1 to 4.5.3) are shown in Table 4.5.1. The values of the temperature contrast obtained in the dry model experiments without the Himalayas are considerably smaller than those in the wet and dry model experiments with the Himalayas as far as the upper tropospheric levels (above 700 mb) are concerned. The absence of the easterly jet in the experiments without the Himalayas is due to the absence of strong thermal winds in the upper troposhere, i.e. between 300 and 100 mb. For example, at 208 mb the temperature contrast is only 0.3 and 0.4° C in the experiments without the Himalayas as against 13.2, and 11.0° C in the experiments with the Himalayas. The models considered without the Himalayas, therefore, lead

Table 4.5.1 : Ocean-continent temperature contrast (ΔT °c) between 2.5° N and 27.5° N

Level K	Pressure mb	With the Himalayas with sea surface temperature at 300° K		Without the Himalayas with sea surface temperature at	
		Wet Model	Dry Model	300° K	290° K
9	Surface	13.2	33.2	21.9	29.4
8	955	8.1	22.1	9.9	13.8
7	855	5.1	11.2	4.7	6.4
6	710	4.1	3.7	0.7	1.0
5	540	4.0	3.1	0.4	0.5
4	367	11.2	1.4	·0.3	0.9
3	208	13.2	11.0	0.3	0.4
2	82	- 13.0	-11.6	0.3	0.4
1	10	- 1.4	2.3	0.6	0.9

to the inferrence that the monsoon circulation as observed cannot be simulated until the northsouth temperature contrast on the mean attains a value of not less than 0.5° C per degree latitude in the upper troposphere.

It is also seen from Table 4.5.1 that the ocean-continent temperature contrast below 850 mb in the dry model experiments is large (more than twice, in some cases) as compared to what it is in the wet model experiment. The main reason for this is that in the dry model experiment the process of evaporation, which acts as a heat sink, is missing and hence the entire available heat is used up in warming the atmosphere. The presence of moisture would, on one hand, tend to decrease the temperature of the lower layers through evaporation and, on the other hand, increase the temperature of the middle troposphere through condensation. In the following experiments, the role of moisture in the monsoon circulations has been examined.

4.5.4 Wet model without the Himalayas

The presence of moisture in the air is taken into account but not the presence of the Himalayas. Three cases have been considered as already stated :
(a) water vapour mixing ratio at the surface is 80% ($\beta = 0.8$ in equation 4.4.1) of the saturation mixing

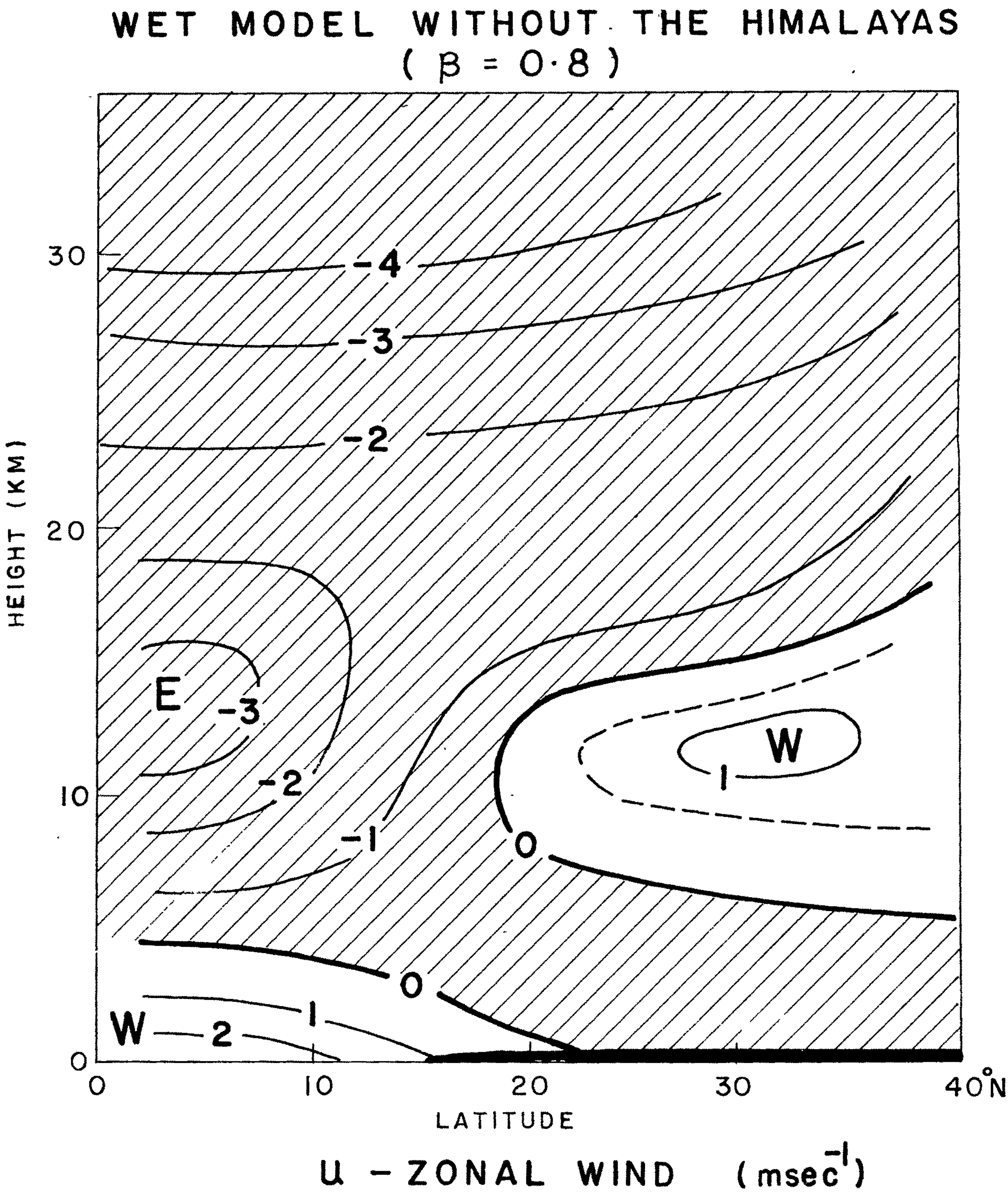

Figure 4.5.10 Vertical cross section of simulated zonal wind (m sec^{-1}) along 80 E fro wet model without the Himalayas with = 0.8. Easterly (E) regime is hatched.

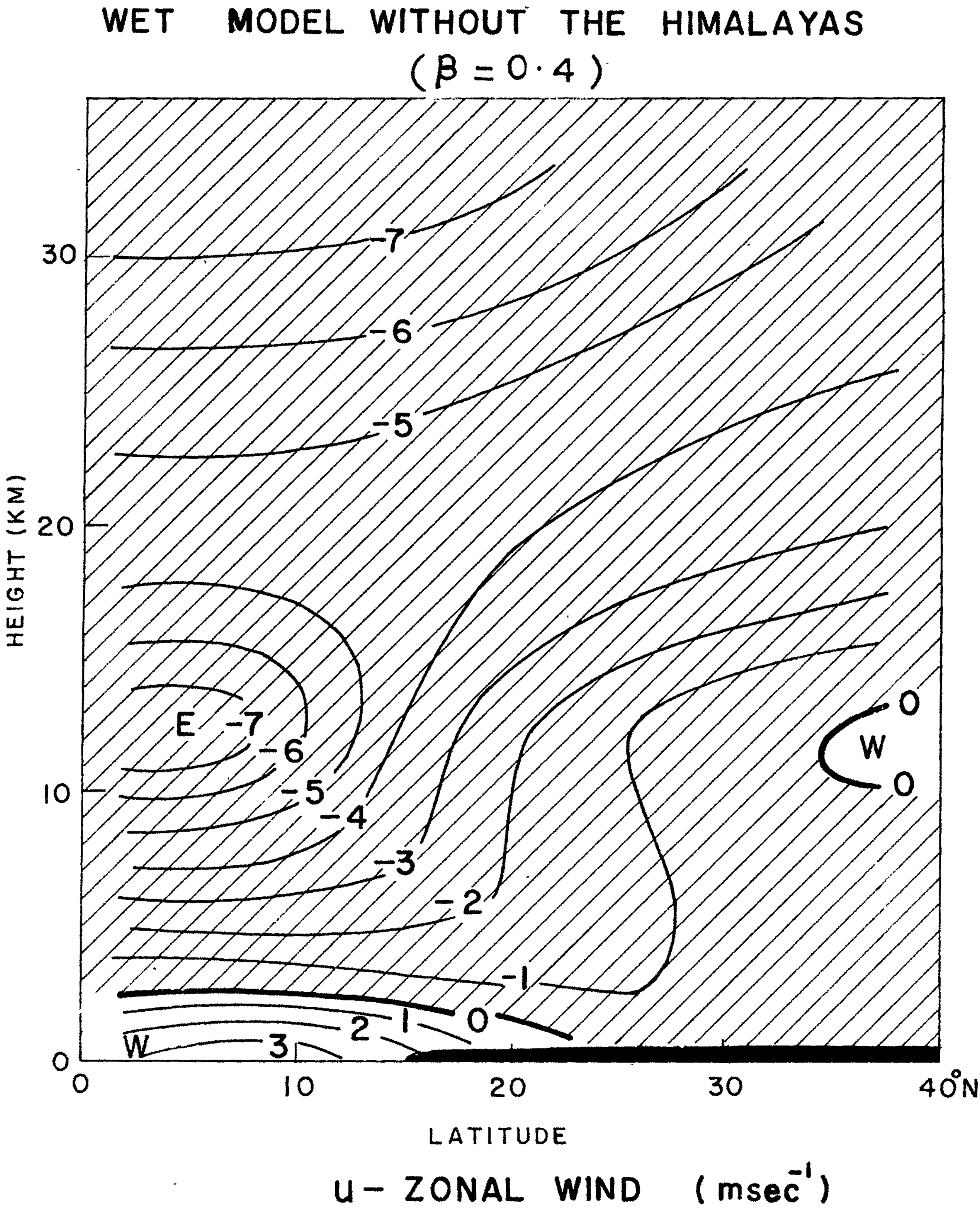

Figure 4.5.11 Vertical cross section of simulated zonal wind (m sec^{-1}) along 80 E fbr wet model without the Himalayas with = 0.4. Easterly regime (E) is hatched.

ratio at the surface, (b) water vapour mixing ratio is 40 % (β = 0.4 in equation 4.4.1) of the saturation mixing ratio at the surface, and (c) condensation occurs at 80 % relative humidity instead of at 100 % with the evaporation rate remaining as in (b). In experiments (a) and (b), condensation is assumed to take place only at 100 % relative humidity.

(a) Surface mixing ratio at 80 % : In Figure 4.5.10 is shown the vertical cross section of the simulated zonal wind. The monsoon circulation generated is weak as compared to that generated in the case of dry model without the Himalayas (Figure 4.5.8). The upper-level easterly decreases from 8 m sec^{-1} in the dry model to 3 m sec^{-1} in the present wet model while the low-level westerly decreases from 3 m sec^{-1} to 2 m sec^{-1}.

(b) Surface mixing ratio at 40 % : The results obtained are presented in Figure 4.5.11. The circulation becomes strong as compared to what it is for β = 0.8 (Figure 4.5.10). The upper-level easterly increases to 8 m sec^{-1} and the low-level westerly to 3 m sec^{-1} as in the dry model without the Himalayas (Figure 4.5.8).

The features noticed as in (a) and (b) may be accounted for as follows. More injection of moisture from the ground (β = 0.8) as in (a) demands more absorption of latent heat of vaporization which, in effect, inhilits building up of ocean-continent temperature contrast (vide Table 4.5.2). Such a build-up is one of the factors responsible for the development of strong circulation. In addition, more moisture content injected into the air from the ground (when $\beta = 0.8$) does not guarantee correspondingly more release of latent heat of condensation in the middle troposphere (vide Table 4.5.3). But when $\beta = 0.4$ as in (b), the less evaporation rate consequent at the ground favours building up of strong ocean-continent temperature contrast (Table 4.5.2). The circulation in (b), therefore, becomes stronger.

The results of the experiments (a) and (b) above are also of fundamental importance in that they explain the well known observational fact, namely, why there is no monsoon-type circulation over the Pacific and the Atlantic. The differential distribution of land and sea in the north-south as over the Indian ocean longitudes is not present over the longitudes of the Pacific and the Atlantic. Since the evaporation rate which is maximum over the oceans, does not differ appreciably from north to south, the necessary north-south temperature contrast for the monsoon-type circulation never builds up over these regimes.

(c) Condensation at 80% relative humidity : It is known that condensation in the atmosphere takes place

Table 4.5.2 : Ocean-continent temperature contrast (ΔT °C)
between 2.5°N and 27.5°N

Level K	Pressure mb	Wet model			
		with the Himalayas R.H. 100% $\beta = 0.8$	Without the Himalayas		
			R.H. 100% $\beta = 0.8$	R.H. 100% $\beta = 0.4$	R.H. 80% $\beta = 0.4$
9	Surface	13.2	5.6	15.1	14.8
8	955	8.1	1.8	7.8	5.7
7	855	5.1	1.8	3.8	3.4
6	710	4.1	0.1	0.8	0.9
5	540	4.0	- 0.2	0.6	0.6
4	367	11.2	- 0.7	0.5	0.5
3	208	13.2	- 0.2	- 0.2	- 0.4
2	82	- 13.0	0.9	0.7	0.7
1	10	- 1.4	0.7	0.6	0.7

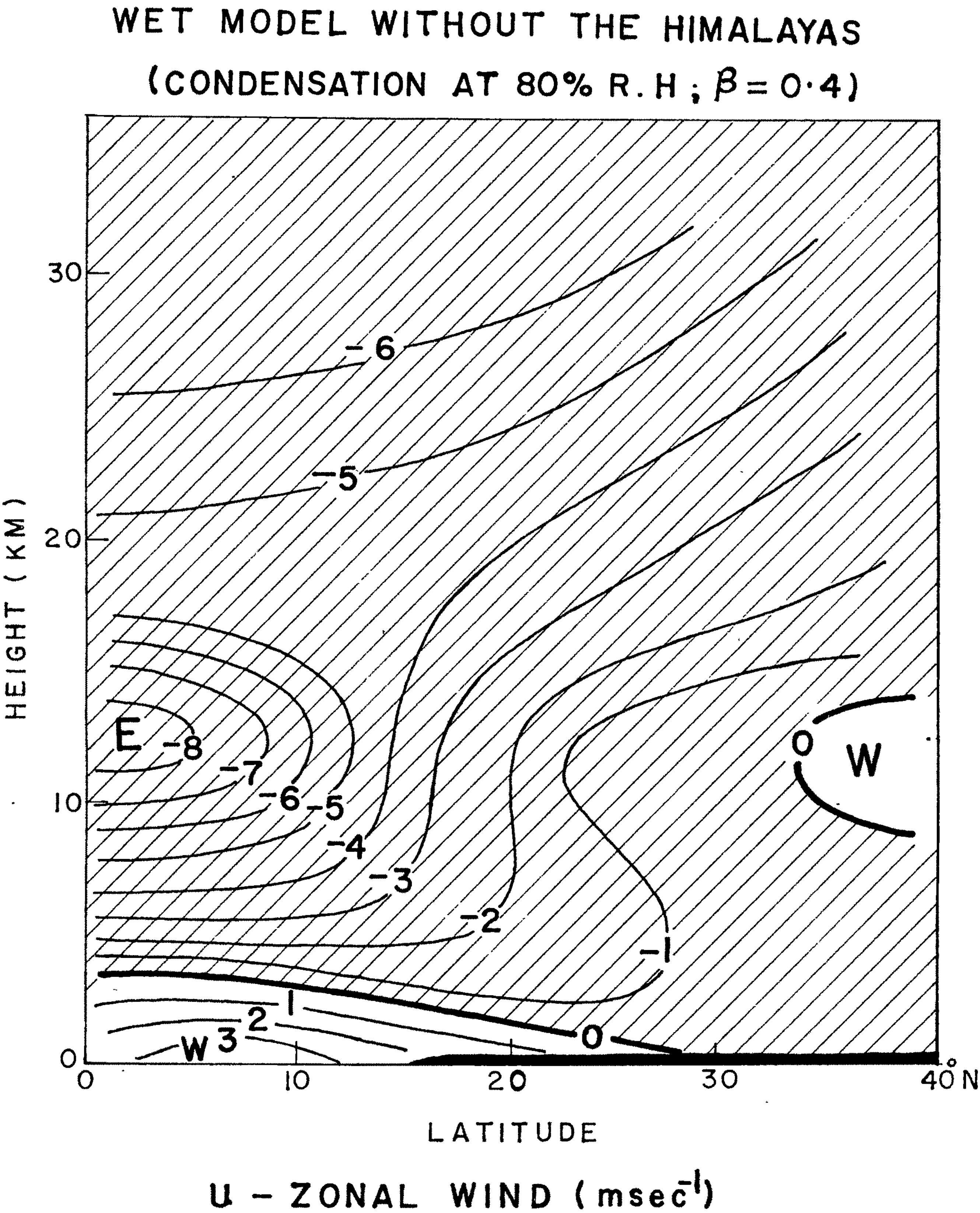

Figure 4.5.12 Vertical cross section of simulated zonal wind (m sec^{-1}) along 80 E for wet model without the Himalayas with condensation at 80% r.h. and = 0.4. Easterly (E) regime is hatched.

well before 100% relative humidity is actually reached. Following Smagorinsky et al (1965), the condensation criterion was set to 80% instead of 100% relative humidity. This would help reduce the allowed storage of water vapour in the free atmosphere and consequently release additional amount of condensation heat.

Figure 4.5.12 shows the simulated zonal wind pattern. The results point out that the monsoon circu--lation with condensation criterion of 80% relative humidity (Figure 4.5.12) remains practically unchanged from that with condensation criterion of 100% relative humidity (Figure 4.5.11). On the contrary, the circulation in Figure 4.5.12 shows an indication of slight weakening when compared to that in Figure 4.5.11. It may be noted that Miyakoda et al (1969) in their two week prediction experiment also arrived at a similar result, namely, that the tropical Hadley Cell is weaker with a condensation criterion of 80% humidity.

4.5.5 <u>Role of evaporation and condensation</u>

Quantitative information about precipitable water from equator to north pole and precipitated water from equator to 42.5°N and also from equator to north pole as obtained in the process of the foregoing wet model experiments is presented in Table 4.5.3. It is seen that the precipitable water in the models with

Table 4.5.3 : Precipitable water and precipitated water for wet model experiments. The values represent integrated amount from the surface to the top of the atmosphere.

	With the Himalayas R.H.100% $\beta = 0.8$	Without the Himalayas		
		R.H.100% $\beta = 0.8$	R.H.100% $\beta = 0.4$	R.H.80% $\beta = 0.4$
Precipitable water Equator to north pole 10^{16} gm/ longitude	268	263	231	248
Precipitated water Equator to 42.5°N 10^{16} gm/day	0.11958	0.00709	0.02192	0.01832
Precipitated water Equator to north pole 10^{16} gm/day	0.15067	0.00717	0.02982	0.02216

$\beta = 0.8$ is more than that with $\beta = 0.4$ which is consistent. What is more interesting is the fact that the total amount of condensate (precipitated water) became less for the condensation criterion at 80 % relative humidity (0.01832×10^{16} gm) than at 100 % (0.02192×10^{16} gm). It is this feature which is responsible for the lower values obtained of the ocean-continent temperature contrast at 80 % relative humidity than at 100 % (Table 4.5.2), and consequently weakening the circulation (Figure 4.5.12). Table 4.5.3 also reveals that the total amount of condensate is less for higher evaporation rate (vide figures in columns 3 and 4 against precipitated water). The lower values of the ocean-continent temperature contrast obtained with $\beta = 0.8$ than with $\beta = 0.4$ (Table 4.5.2) and the resulting weakening of circulation (Figure 4.5.10) are due to this feature.

The value obtained for the total amount of condensate in the model with the Himalayas (0.11958×10^{16} gm) which is about five times more than those in the other models without the Himalayas speaks about the dominant role of the Himalayas in the shaping of rainfall and circulation patterns of the Indian summer monsoon.

4.5.6 Role of moisture

The wet and dry model experiments conducted with and without the Himalayas point out that the circulation as obtained by introducing moisture into the atmosphere (Figure 4.5.11) is not very different from that as obtained without moisture (Figure 4.5.8). In other words, the addition of moisture into the dry air may not be considered as an important factor for the development of the monsoon circulation although it is very essential for the incidence of rainfall.

REFERENCES

Charney, J.	1959	On the General Circulation of the Atmosphere. The Atmosphere and Sea in Motion. Oxford Univ.Press.
Flohn, H.	1960	Recent Investigations on the Mechanism of the Summer Monsoon of Southern and Eastern Asia. The Monsoons of the World. India Met. Dept. New Delhi. pp.75-88.
Flohn, H.	1964	Investigations on the Tropical Easterly Jet. Meteor. Inst. Der, Univ. Bonn., Heft 4. 83 pp.
Koteswaram, P.	1960	The Asian Summer Monsoon and the General Circulation over the Tropics. The Monsoons of the World. India Met. Dept. New Delhi pp. 105-110.
Koteswaram, P.	1969	Forecasting of Upper Winds and Temperature in Tropical latitudes, with special Reference to Jet Streams Aeronautical Met.Tech.Note No.95; WMH-no. 227 TP 121. pp. 218-228.
Leith, C.	1965	Numerical Simulation of the Earth's Atmosphere. Methods in computational Physics 4.Academy Press.N.Y.

London, J., G. Ohring, I. Ruff.	1956	Radiative Properties of the Stratosphere Final Rep.Res.Div., College of Engineering. N.Y.Univ. 48 pp.
Manabe, S., F. Moller	1961	On the Radiative Equilibrium and Heat Balance of the Atmosphere. Mon. Wea. Rev. 89. pp. 503-532
Manabe, S., Smagorinsky, J. R.F. Strickler	1965	Simulated Climatology of a General Circulation Model with a Hydrologic Cycle. Mon.Wea.Rev.93 pp.769-798.
Manabe, S., J.L. Holloway Jr., H.M. Stone	1970	Tropical Circulation in a time-integration of Global Model of the Atmosphere. J.Atmos.Sci.27. pp.580-613
Mintz, Y.	1965	The Seasonal Variations in a numerical General Circulation experiment. Proc.Int.Symp.on large-scale processes. Moscow.
Mintz. Y., A. Arakawa.	1963	Long-term Numerical Integration of the Equations of Atmospheric Motions over the Entire Globe. Proc.Int. symp.on Dynamics of Large-scale Processes. Boulder.
Miyakoda, K., J. Smagorinsky, R.F.Strickler, G.D.Hembree	1969	Experimental Extended Predictions with a Nine-level Hemispheric Model. Mon.Wea.Rev.97 pp.1-76.
Murgatroyd, R.J.	1964	Ozone and Water Vapour in the Upper Troposphere and Lower Stratosphere. W.M.O. Tech.Note 169. TP 83. pp. 68-69.

Phillips, N.	1956	The General Circulation of the Atmosphere. A numerical Experiment. Quart.J.Roy.Met.Soc.82. pp. 123-164.
Ramanathan, K.R., R. N. Kulkarni	1960	Mean Meridional Distribution of Ozone in Different Seasons Calculated from Umkher Observations and Probable Vertical Transport Mechanism. Quart.J.Roy.Met.Soc. 86. pp. 151-155.
Smagorinsky, J.	1963	General Circulation Experiments with the Primitive Equations : I. The Basic Experiment. Mon.Wea.Rev.91. pp. 99-164.
Smagorinsky, J., S. Manabe, J.L. Holloway Jr.	1965	Numerical Results from a Nine-level General Circulation Model of the Atmosphere.Mon.Wea. Rev.93. pp.727-768.
U.S. Air Force	1962	U.S.Standard Atmosphere, 1962. Govt. Printing Office. Washington.